# Enzyme Nanoscale Interactions with Manganese Zinc Sulfide Give Insight into Potential Antiviral Mechanisms and SARS-CoV-2 Inhibition

Robert K. DeLong,* Hanah Huber, Cesar Aparicio-Lopez, Abeera Bhatti, Ryan Swanson, Tej B. Shrestha, and Natasha N. Gaudreault

Read Online

ACCESS | Metrics & More | Article Recommendations | Supporting Information

**ABSTRACT:** Recent interest in nanomedicine has skyrocketed because of mRNA vaccine lipid nanoparticles (LNPs) against COVID-19. Ironically, despite this success, the innovative nexus between nanotechnology and biochemistry, and the impact of nanoparticles on enzyme biochemical activity is poorly understood. The studies of this group on zinc nanoparticle (ZNP) compositions suggest that nanorod morphologies are preferred and that ZNP doped with manganese or iron can increase activity against model enzymes such as luciferase, DNA polymerase, and $\beta$-galactosidase ($\beta$-Gal), with the latter previously being associated with antimicrobial activity. SARS-CoV-2 encodes several of these types of oxido-reductase, polymerase, or hydrolase types of enzymes, and while metamaterials or nanoparticle composites have become important in many fields, their application against SARS-CoV-2 has only recently been considered. Recently, this group discovered the antiviral activity of manganese-doped zinc sulfide (MnZnS), and here the interactions of this nanoparticle composite with $\beta$-Gal, angiotensin converting enzyme (ACE), and human ACE2 (hACE2), the SARS-CoV-2 receptor, are demonstrated. Low UV, circular dichroism, and zeta potential results confirm their enzyme interaction and inhibition by fluorometric area under the curve (AUC) measurements. The $IC_{50}$ of enzyme activity varied depending on the manganese percentage and surface ranging from 20 to 50 $\mu$g/mL. MnZnS NPs give a 1−2 log order inhibition of SARS-CoV-2; however, surface-capping with cysteine does not improve activity. These data suggest that Mn substituted ZNP interactions to hACE2 and potentially other enzymes may underlie its antiviral activity, opening up a new area of pharmacology ready for preclinical translation.
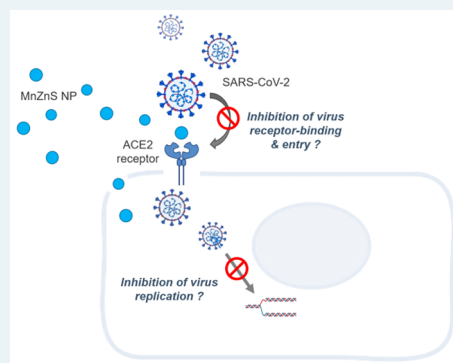
**KEYWORDS:** nanoparticle, antiviral, SARS-CoV-2, zinc, manganese, capped/doped

Although the nanomedicine research wave may be peaking,[1,2] the impact of nanoparticles on enzyme biochemical activity remains largely uninvestigated. In general, enzymes are classified according to the type of biochemical reaction they catalyze, including (1) transferases, which transfer a functional group such as a phosphate to a substrate, (2) oxidoreductases, which catalyze the oxidation or reduction of a substrate, (3) hydrolases, which catalyze hydrolysis or dehydration reactions, (4) ligases, which join two molecules or functional groups together to form a covalent bond, (5) isomerases, which catalyze isomerizations, and (6) lyases, which tend to exchange substituents. A variety of different proteins and enzymes are associated with disease and thus the identification of specific nanoparticle pharmacologic inhibitors has become extremely important.

A great deal of work by the authors' lab and many others supports the interaction of zinc oxide nanoparticles (ZnO NPs) to proteins.[3,4] Early model biochemical studies focused on the luciferase (Luc) enzyme which combines both transferase and oxido-reductase activity; the exquisite sensitivity of its bioluminescence reaction makes it ideal for measuring the effects of nanoparticle enzyme activation or inhibition.[5,6] ZnO NP activity against drug-resistant bacteria was shown to be shape-dependent and to correlate with the inhibition of a specific class of hydrolase enzyme, $\beta$-galactosidase ($\beta$-Gal).[7] Another example is targeted medicines against cancer kinases that have been developed, and it has been shown that treating cancer cells or injecting melanoma tumors in mice with ZnO NPs inhibits the phosphorylation of some of these cancer-related kinases.[8,9]

Therefore, the shape and compositional dependence for zinc nanoparticle (ZNP) enzyme biochemical activity is perhaps one of the most important new areas of antiviral inhibitors. Most recently, a second generation ZNP chemistry was

reported, zinc sulfide doped with manganese (MnZnS) and alternatively iron (FeZnS) were reported to have 2log order inhibition of $\beta$-Gal and were capable of inhibiting porcine reproductive and respiratory syndrome virus (PRRSV).[10] Here, the interactions of MnZnS to $\beta$-Gal, human angiotensin converting enzyme (ACE), and hACE2 were compared, along with effects on biochemical activity and inhibition of SARS-CoV-2.

## ■ MATERIALS AND METHODS

**Materials.** Au NPs, B$_4$C, Si$_3$N$_4$, CaCO$_3$, and SiO$_2$ NPs were obtained from commercial sources, either Sigma-Aldrich (St. Louis, MO) or PlasmaChem GmbH (Berlin, Germany). The synthesis of defined nanorod to nanosphere ZnO and their characterization by transmission electron microscopy (TEM) has been previously described.[11] Synthetic methods for shape-controlled nanorod (NR) morphologies defined percentage (1, 3, 5 and 10%) iron or manganese into zinc oxide or sulfide were also recently described.[10,12,13] Cysteine capping of Mn/ZnS was accomplished as follows. The MnZnS pellet was ground to create a fine powder. An mount of 3 g of Mn/ZnS was dissolved in 5 mL of DI water. Then, 3 g of L-cysteine was dissolved in 2 mL of DI water. The pH was adjusted to 7 using pH strips and 0.1 M NaOH. Then, the Mn/ZnS solution was mixed with the L-cysteine solution, and the final mixture was allowed to stir overnight. The Mn/ZnS suspension turned into a clear white solution. Next, the material was centrifuged at 4000 rpm for 5 min. The supernatant was discarded, and the precipitate was resuspended in water. This cycle was completed three times. After the final centrifugation, the precipitate was left to dry. Characterization was by Fourier transform infrared (FTIR) spectroscopy where pure L-cysteine was obtained and the spectra showed a NH$_2$ peak, SH peak, and COOH peak. Another FTIR measurement was taken after the conjugation of L-cysteine to the nanoparticle. The latter showed the disappearance of the SH group. The spectra were compared to the literature, and the results agreed with a thiol interaction between nanoparticle and L-cysteine.

**Biochemical Enzyme Assays.** These experiments were conducted similarly to those in our previous studies.[5,6] A 0.1 mg/mL stock solution of luciferase was created using PBS buffer. A stock solution of 1 mg/mL of each ZnO morphology NR:NP ratio was created using Millipore H$_2$O. ZnO:luciferase mixtures were created by mixing 10 $\mu$L of 0.1 mg/mL luciferase with 10 $\mu$L of 1 mg/mL ZnO. This was performed separately for each ZnO morphology. A luciferase only control was created by incubating 10 $\mu$L of 0.1 mg/mL luciferase with 10 $\mu$L of Millipore H$_2$O. All mixtures were allowed to incubate for 10 min at room temperature. Aliquots of 4 $\mu$L of each mixture were added to wells in an opaque 96-well plate in triplicate, 100 $\mu$L of Promega substrate mix was then added to each well , and luminescence was measured using a FLUOstar OPTIMA microtiter plate reader over time. Averages were calculated in quadruplicate, and a best-of line was generated using all data points for the kinetics experiment. Similar experiments were conducted for the rapid kinetics experiments. MONP screening experiments with B$_4$C and Si$_3$N$_4$ as controls were performed in triplicate or quadruplicate and were repeated twice by two independent investigators, and the standard deviation was calculated. For $\beta$-galactosidase assays, a stock solution of commercial grade ZnO (Sigma-Aldrich) was prepared by suspending 2 mg of metal oxide or other nanoparticles in 1 mL of Millipore H$_2$O for a stock

concentration of 2 mg/mL. The $\beta$-galactosidase enzyme (Sigma-Aldrich) was diluted using Millipore H$_2$O to create a stock solution of 1 mg/mL concentration. Mixtures of $\beta$-galactosidase with ZnO and other nanomaterials were prepared by incubating 10 $\mu$L of $\beta$-galactosidase, 100 $\mu$L of ZnO solution, and varied concentrations of substrate, ranging from 12.5 to 100 $\mu$L at 37 °C for 30 min. The colorimetric substrate used is ortho-nitrophenyl-$\beta$-galactoside (ONPG), and the fluorescent substrate is 4-methylumbelliferyl $\beta$-D-galactopyranoside (MUG). Both ONPG (Sigma-Aldrich) and MUG (Sigma-Aldrich) were used as substrates for initial absorbance and fluorescence screening experiments, respectively. A $\beta$-galactosidase control was prepared by incubating 10 $\mu$L of $\beta$-galactosidase, 100 $\mu$L of Millipore H$_2$O, and varied concentrations of ONPG (12.5−100 $\mu$L) at 37 °C for 30 min. After incubation, 50 $\mu$L of Na$_2$CO$_3$ (Sigma-Aldrich) was added to each mixture. Sample aliquots of 100 $\mu$L of each mixture and the $\beta$-galactosidase control were then placed into a 96-well plate in triplicate. Absorbance of the nitrophenyl product was measured at 485 nm using a FLUOstar OPTIMA microtiter plate reader. The fluorescence of the methylumbelliferyl galactoside product was measured at 360/445 nm using a Molecular Devices microtiter plate reader. The average and standard deviation of the four triplicates were used to graph the results. The ACE activity assay was conducted very similarly. The working stock of ACE enzyme (Sigma-Aldrich, St. Louis, MO) was 0.1 units dissolved in 100 $\mu$L of 1× PBS buffer. BRAND 96-well black, clear flat bottom plates were used. The 2.5 mM substrate solution was prepared by adding 1.875 $\mu$L of fluorometric substrate and diluting with 75 $\mu$L of 1× PBS buffer. ACE enzyme (2.5 uL) was also added into the substrate. A concentration of 50 $\mu$g/$\mu$L MnZnS NPs (1%, 3%, and 5%, both uncapped and capped) was added separately in the same wells with enzyme and substrate. Separate wells of 2.5 mM substrate, 2.5 $\mu$L of enzyme only (with the total volume of 130 $\mu$L), and 130 $\mu$L of 1× PBS buffer without nanoparticles were used as controls. Fluorometric readings were taken on a Synergy H1 instrument (Winooski, VT, USA) with the settings of fluorescence spectrum, fixed excitation 360 nm, and emission 400−700 nm in 10 nm steps while the temperature was 37 °C. Background was subtracted for the NP alone controls. The area under the curve (AUC) was calculated for enzyme+substrate and samples containing 1%, 3%, and 5% (both uncapped and capped) NPs using the formula, (Y1 + Y2)/2 × (X2 − X1), where X1 = 400 wavelength, X2 = 410 wavelength, Y1 is the RFU at 400 wavelength, and Y2 is the RFU at 410 wavelength. The same process was repeated for each wavelength and corresponding RFU to get each AUC. (RFU = relative fluorescence units.) All the AUCs were then summed to obtain the total area under the curve for each concentration. The $P$ value for each NP type was also calculated, in comparison with the value of enzyme+substrate. IC$_{50}$ (% inhibition) values for each type and concentration were also calculated from the AUC values and their standard deviations were calculated as well.

**Circular Dichroism (CD) Spectra.** Soluble ACE2-Fc fusion protein (Invivogen) in the amount of 50 $\mu$g was suspended in 500 $\mu$L of LAL water to create a 0.1 $\mu$g/$\mu$L hACE2 stock. An amount of 10 mg of 3% MnZnS NPs was suspended in 1 mL of deionized water to create a 10 $\mu$g/$\mu$L NP stock. A control spectrum was obtained using 300 $\mu$L of hACE2 stock. The sample was then recovered from the CD cuvette, and 3 $\mu$L of NP stock was added to create a 1:1 mass-

## A) 1% MnZnS Voltage



## B) 3% MnZnS Voltage



## C) 5% MnZnS Voltage
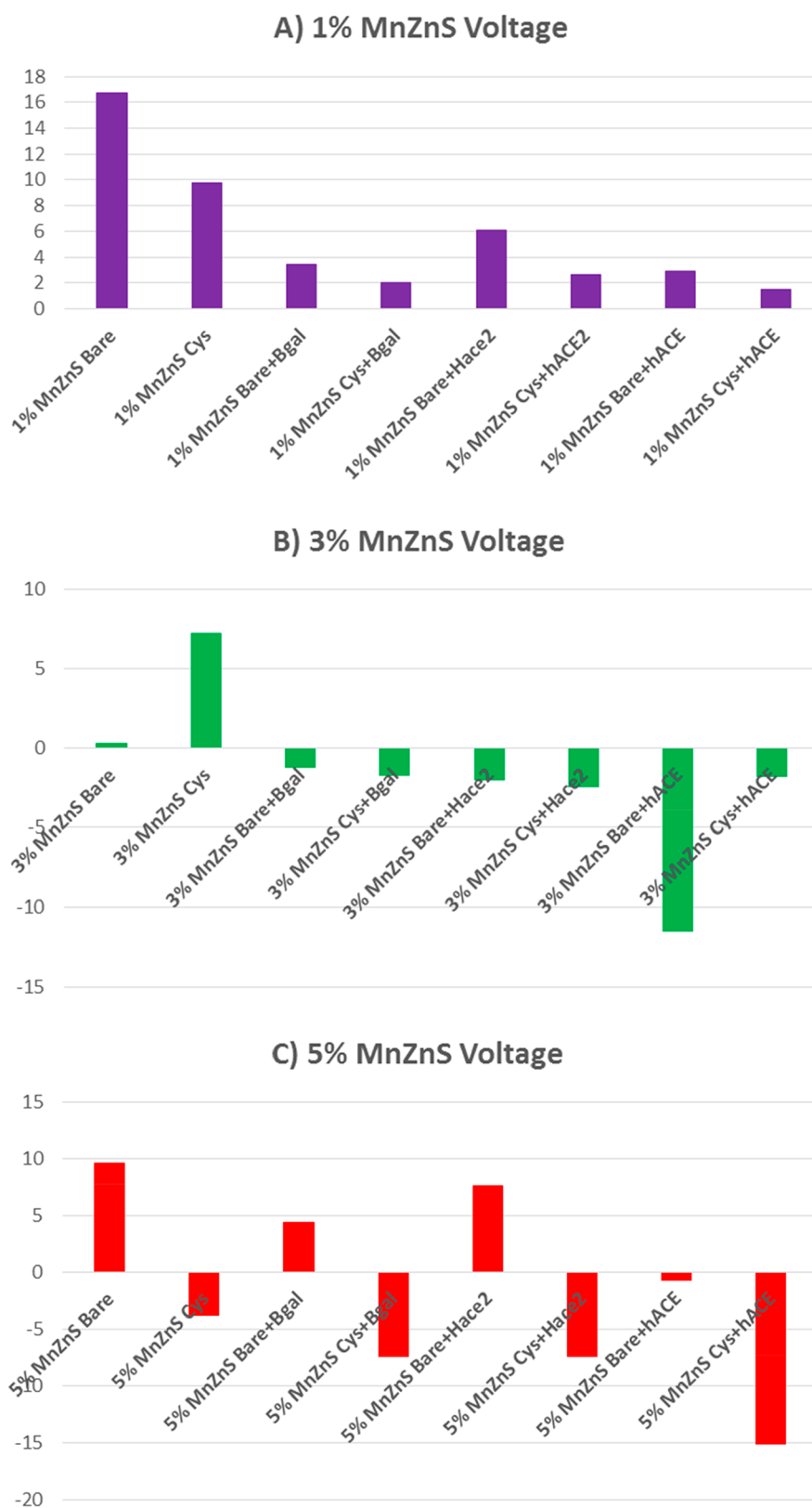


**Figure 1.** Zeta potential measurements for MnZnS nanoparticle interaction with $\beta$-Gal, angiotensin converting enzyme (hACE), and human ACE2 (hACE2) for 1% MnZnS (A), 3% MnZnS (B), and 5% MnZnS (C). $y$-axis units, millivolts

to-mass ratio. The sample was incubated at room temperature on an orbital shaker at 50 rpm for 30 min. After the incubation period, 5 $\mu$L of the sample was saved for UV−vis spectra collection. CD spectra were obtained using the rest of the sample, which was once again recovered from the cuvette after data collection. An additional 12 $\mu$L of NP stock was added to
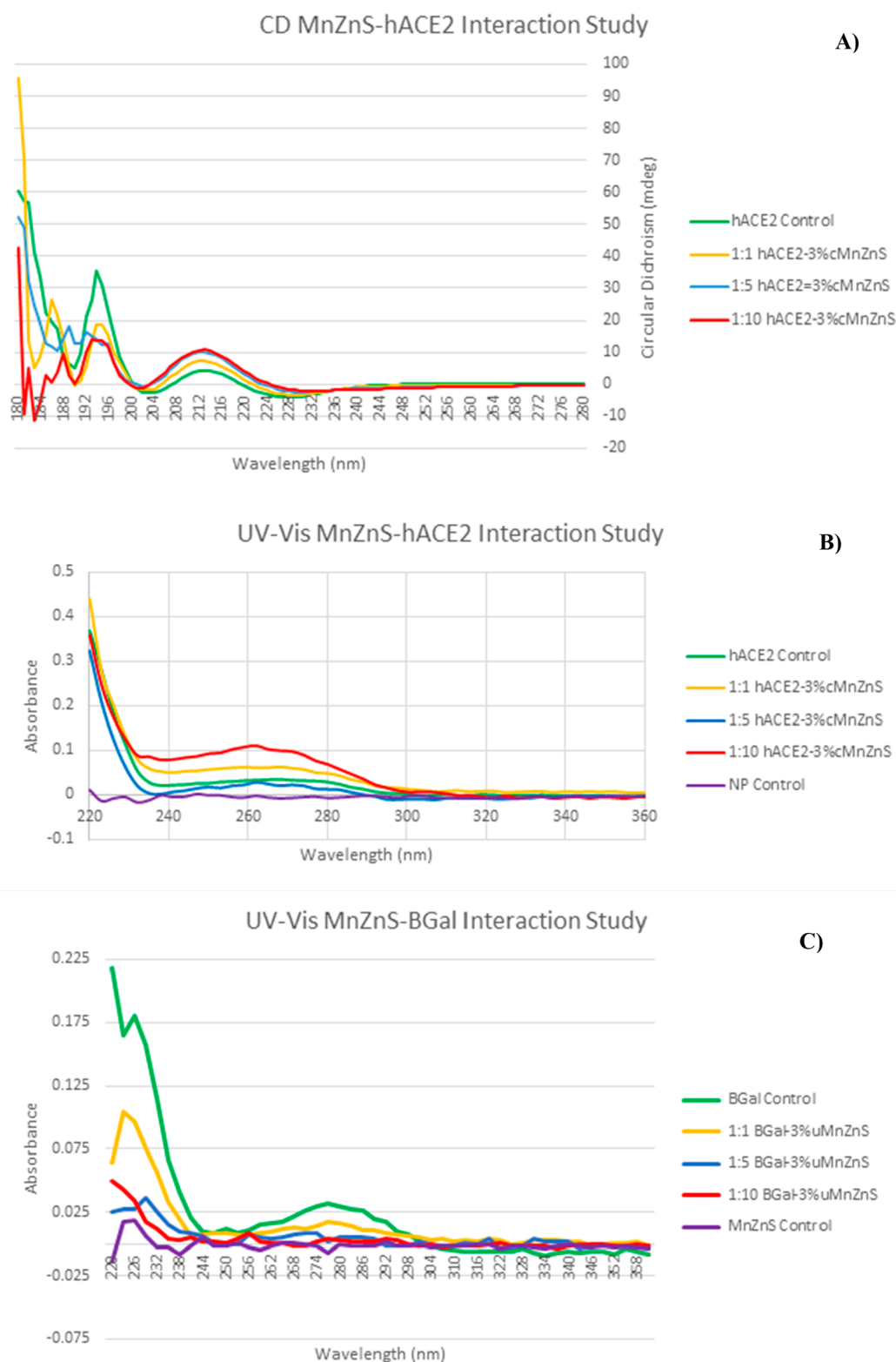
**Figure 2.** Changes in hACE2 protein secondary structure upon interaction to MnZnS. All ratios are reported as protein:MnZnS. (A) CD spectrum of the effect of 3% MnZnS NRs capped with cysteine on hACE2 at mass-to-mass ratios of 1:1 (yellow), 1:5 (blue), and 1:10 (red). (B) UV−vis spectrum of the effect of 3% MnZnS NRs capped with cysteine on hACE2 at mass-to-mass ratios of 1:1 (yellow), 1:5 (blue), and 1:10 (red). (C) UV−vis spectrum of the effect of bare 3% MnZnS NRs on β-galactosidase at mass-to-mass ratios of 1:1 (yellow), 1:5 (blue), and 1:10 (red).

the sample (1:5 mass-to-mass ratio) and allowed to incubate for an additional 30 min at room temperature with shaking at 50 rpm. A 5 μL aliquot of the sample was set aside for UV−vis

spectra collection before the remainder was used for CD spectra collection. After recovering the sample, 15 μL of NP stock was added (1:10 mass-to-mass ratio) before the sample

was incubated once again. Before collecting the final set of CD spectra, 5 $\mu$L of the 1:10 sample was saved for UV–vis spectra collection. CD spectra were collected in the 180–280 nm range using a 1 mm path length quartz cell at ambient temperature. The samples were scanned with a step size of 1.0 nm, bandwidth of 1.0 nm, and rate of 0.5 s per point. Spectra were collected in triplicate and processed by background subtraction, averaging, and smoothing using Pro-Data Viewer software from AppliedPhotophysics.

**UV–Vis Spectra (hACE2).** The samples set aside during CD spectra collection were analyzed using UV–vis spectroscopy. A total of 1.5 $\mu$L of each sample was loaded onto pedestals before spectra were collected in the 220–750 nm range using NanoDrop 8000 standard UV–vis settings.

**UV–Vis Spectra ($\beta$-Galactosidase).** An amount of 10.1 mg of $\beta$-galactosidase (Sigma-Aldrich) was dissolved in 2 mL of deionized water to create a 5.05 mg/mL solution. Then 300 $\mu$L of the 5.05 mg/mL $\beta$-galactosidase solution was added to 700 $\mu$L of water to create a 1.5 $\mu$g/$\mu$L $\beta$-galactosidase stock solution. An amount of 1.5 mg of bare (uncapped) 3% MnZnS NPs was suspended in 1.5 mL of deionized water to create a 1.5 $\mu$g/$\mu$L 3% uMnZnS (uncapped MnZnS) NP stock solution. Then 100 $\mu$L of $\beta$-galactosidase stock was added to a 2 mL Eppendorf tube, along with 100 $\mu$L of 3% uMnZnS stock to create a 1:1 mass-to-mass ratio of $\beta$-galactosidase to 3% uMnZnS. Tube contents were gently mixed by inverting the tube several times before being incubated at room temperature on an orbital shaker at 50 rpm for 30 min. After the incubation period, 5 $\mu$L of the mixture was set aside for spectra collection. A volume of 400 $\mu$L of 3% uMnZnS stock was added to the interaction tube to create a 1:5 mass-to-mass ratio of $\beta$-galactosidase to 3% uMnZnS. The sample was allowed to incubate for an additional 30 min at room temperature, shaking at 50 rpm before another 5 $\mu$L was set aside for spectra collection. Then 500 $\mu$L of 3% uMnZnS stock was added to the interaction tube to create a 1:10 mass-to-mass ratio of $\beta$-galactosidase to 3% uMnZnS. The sample was allowed to incubate for an additional 30 min at room temperature, shaking at 50 rpm before a final 5 $\mu$L was set aside for spectra collection. The samples set aside after each incubation period along with the stock solutions (which would serve as controls) were analyzed using UV–vis spectroscopy. A total of 1.5 $\mu$L of each sample were loaded onto pedestals before spectra were collected in the 220–750 nm range using NanoDrop 8000 standard UV–vis settings.

**MnZnS Effect on SARS-CoV-2 Virus Infection In Vitro.** Vero E6 cells (ATCC; Manassas, VA) were used for virus propagation and titration. Cells were cultured in Dulbecco's Modified Eagle Medium (DMEM, Corning, New York, NY), supplemented with 5% fetal bovine serum (FBS, R&D Systems, Minneapolis, MN) and antibiotics/antimycotics (ThermoFisher Scientific, Waltham, MA), and maintained at 37 °C under a 5% $CO_2$ atmosphere. The SARS-CoV-2/human/USA/WA1/2020 lineage A was acquired from BEI Resources (BEI item #: NR-52281; Manassas, VA). A passage 2 plaque-purified stock of lineage A WA1 was used for this study. Virus stocks were sequenced by next generation sequencing (NGS) using the Illumina MiSeq sequencer, and the consensus sequences were found to be homologous to the original strains obtained from BEI (GISAID accession number: EPI_ISL_404895 (WA-CDC-WA1/2020)). To determine infectious virus titers of virus stocks and experimental samples, 10-fold serial dilutions were performed on Vero E6 cells. The

presence of cytopathic effect (CPE) after 96 h incubation at 37 °C was used to calculate the 50% tissue culture infectious dose ($TCID_{50}$) per milliliter using the Spearman–Kaerber method.

The effect of MnZnS on SARS-CoV-2 virus infection was determined by evaluating virus titers of SARS-CoV-2 infected Vero E6 cells in the presence or absence of MnZnS NPs. Vero E6 cells were seeded to 96-well plates the day prior to use. On the day of assay, the culture media was removed from the Vero E6 cells and replaced with 100 $\mu$L/well of MnZnS NPs diluted in culture media (5, 10, 20, 50, and 100 $\mu$g/mL) or with culture media only as a control. This was followed immediately by the addition of 100 $\mu$L/well of SARS-CoV-2 virus for an approximate 0.01 multiplicity of infection. Three independent experiments were performed, and each experiment included four technical replicates. At 48 h postinfection (hpi), cell culture supernatants were removed and titrated on Vero E6 cells to determine infectious virus titers by $TCID_{50}$ assay as described above. Two-way ANOVA statistical analysis was performed on log transformed virus titer data using GraphPad Prism software, with $p < 0.05$ considered significant.

## ■ RESULTS AND DISCUSSION

Earlier work has suggested that manganese-doped zinc sulfide (MnZnS) could inhibit model enzymes luciferase (Luc) and $\beta$-Gal with an $IC_{50}$ between 20 and 50 $\mu$g/mL.[10] Current dogma suggests that nanoscale interactions with enzymes could cause competitive, uncompetitive, or noncompetitive inhibition. Initially, this shape-dependence was investigated by testing various nanorod to nanosphere ratios[11] on the well characterized ZnO-Luc system,[5,6] demonstrating that nanorods were preferred (Figure S1). Subsequent work showed that substitution with iron, zinc, or manganese in small amounts ($\leq$5%, 3% or 1%)[10] could increase inhibition against Luc (Figure S2) and a dose–response curve comparing 1% MnZnS against Luc and $\beta$-Gal again confirms the $IC_{50}$ is <50 $\mu$g/mL (Figure S3). These data combined with earlier work suggested that MnZnS nanorods would increase enzyme interaction, which was investigated by zeta potential analysis (Figure 1).

Figure 1 shows the interaction of MnZnS with the enzymes $\beta$-Gal, ACE, and another hydrolase enzyme closely related to hACE2, the receptor for SARS-CoV-2. Anionic shifts in the zeta potential were consistent with all percentages of manganese-doping for cysteine-capped or uncapped materials. Although the data consistently show protein-dependent charge shifts as expected, the shift for 3% MnZnS with ACE was dramatic, potentially suggesting a protein conformational rearrangement which was further investigated.

UV and CD spectroscopy can be used to investigate changes in protein secondary structure as a function of binding to nanoparticles.[6] These methods were used to investigate the impact of 3% MnZnS nanoparticle interactions with hACE2 protein (Figure 2).

Figure 2 shows a significant change in hACE2 protein secondary structure upon interaction with MnZnS NRs as reflected in the CD (Figure 2a) and UV (Figure 2b) spectra. The experiment was repeated with $\beta$-Gal and showed a very similar result (Figure 2c). UV of MnZnS:ACE interaction was also conducted (Figure S4).

To assess NP inhibition of biochemical activity, a fluorometric assay was developed to measure angiotensin converting enzyme (ACE) for area under the curve analysis (AUC) as a function of manganese percentage and concentration (Figure 3).

## ACE Activity with Uncapped MnZnS NPs



## 3% MnZnS dose-response
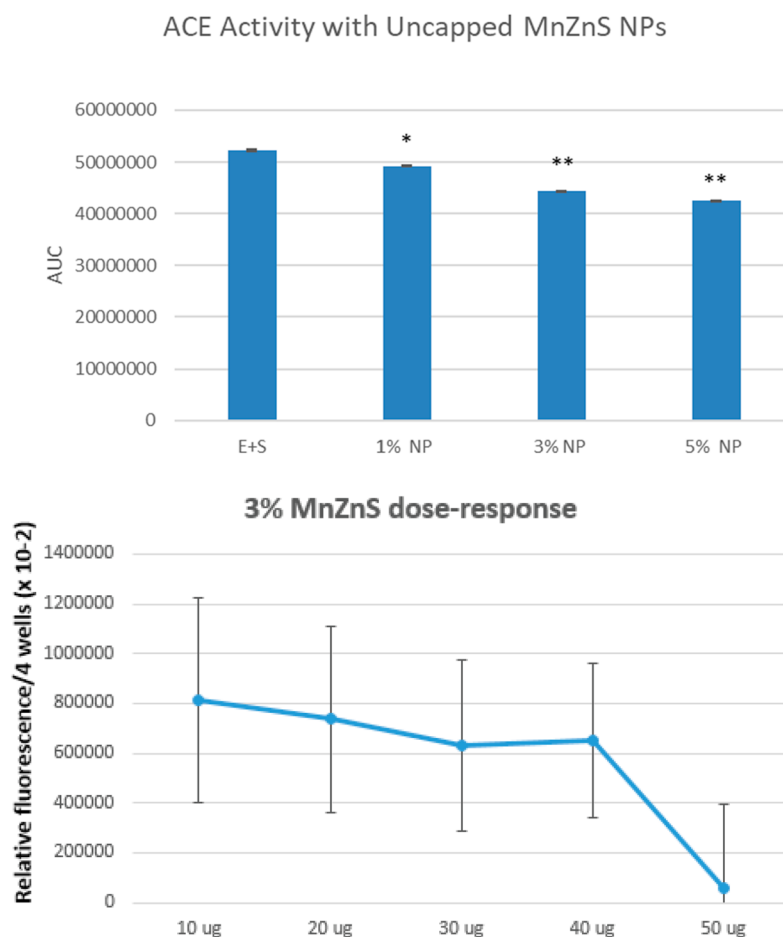


**Figure 3.** Inhibition of ACE biochemical activity by different percentages of MnZnS nanoparticles (top panel). *$p < 0.05$, **$p < 0.01$. Time-point data from 0 to 1 h were combined, and the relative fluorescence produced was plotted for 3% MnZnS NPs at each different input concentration (bottom panel).

As shown in Figure 3, all three manganese dopant percentages resulted in significant inhibition relative to enzyme substrate (E+S) only controls. The 3% and 5% MnZnS showed more significant inhibition. The trend in biochemical activity per dose of nanoparticles also suggests dose-dependence. To further investigate this, the percentage of inhibition at the maximal dose tested, 50 $\mu$g/mL, was tabulated (Table 1).

**Table 1. Percentage of Inhibition at the Maximal Dose Tested[a]**

| composite nanoparticle type | IC$_{50}$ (% inhibition ± SD) |
|---|---|
| 1% uncapped MnZns | 5.82% ± 7.44% |
| 3% uncapped MnZnS | 15.16% ± 1.9% |
| 5% uncapped MnZnS | 18.8% ± 5.44% |
| 1% capped MnZnS | 19.43% ± 2.14% |
| 3% capped MnZnS | 24.52% ± 2.95% |
| 5% capped MnZnS | 20.76% ± 0.8% |

[a]Percent inhibition at 50 ug NP dose input.

The data in both Figure 3 and Table 1 suggest that the nanoparticles inhibit ACE biochemical activity. These data are consistent with previous reports demonstrating MnZnS inhibition of another type of hydrolase, $\beta$-Gal.[10] The nanoparticles were active at or below 50 $\mu$g in-well dosages. For comparison, ACE inhibitors are typically given orally for hypertension management or for heart failure with dosages ranging from 2.5 to 35 mg per day.[14]

Given the biochemical inhibition and interaction with hACE2, it was inferred that these nanoparticle compositions could have antiviral activity against SARS-CoV-2 which was subsequently tested (Figure 4).

The antiviral activity of MnZnS compositions was determined by incubating increasing concentrations of MnZnS in the presence of SARS-CoV-2 on Vero E6 cell cultures. Culture supernatant viral titers at 48 h postinfection showed a statistically significant reduction of virus in the presence of 20 $\mu$g/mL uncapped MnZnS and 50 $\mu$g/mL cys-capped MnZnS (Figure 4A). While there was no significant cytotoxic effect on Vero E6 cultures in the presence of MnZnS up to 20 $\mu$g/mL, cytotoxicity was observed at or above 50 and 100 $\mu$g/mL MnZnS concentrations (Figure 4B; see also Figure S5).

## ■ CONCLUSIONS

Overall, the data suggest that nanorod compositions containing small percentages of manganese and/or iron doped into zinc oxide or especially zinc sulfide interact and have enzyme-specific activation or deactivation with the model enzymes used in this study (Luc, $\beta$-Gal, and ACE). Zeta potential measurements confirm protein interaction with all three enzymes which was especially evident for the 3% MnZnS
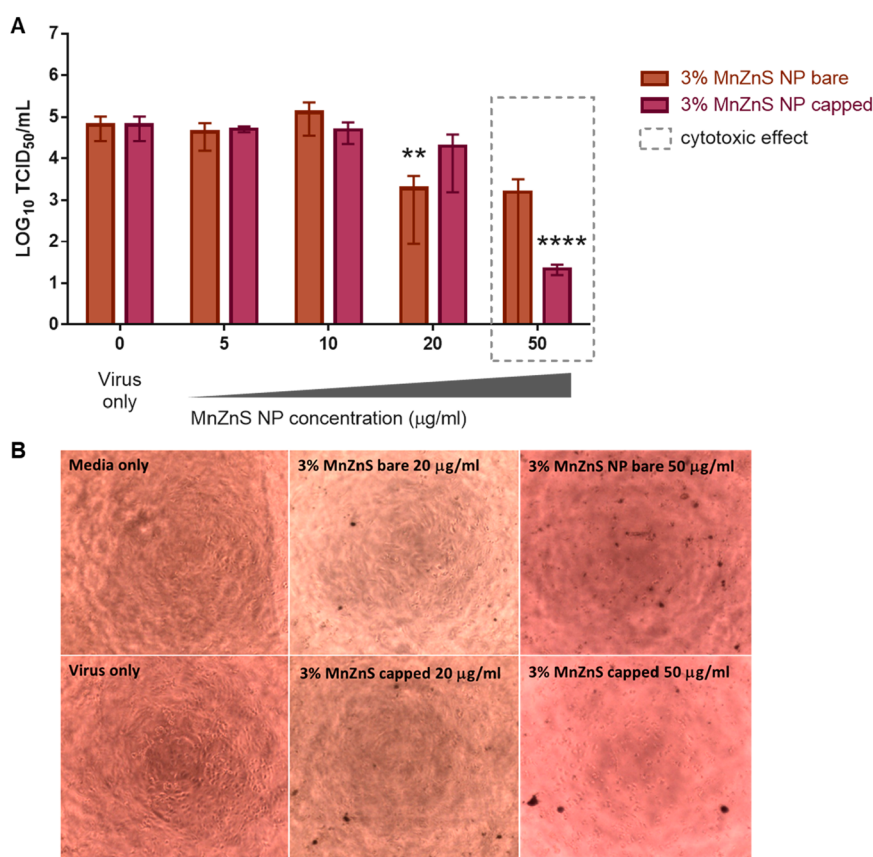
**Figure 4.** (A) Virus titers ($TCID_{50}$/mL) of supernatants collected from Vero E6 cell cultures at 48 h post-treatment with 3% cys-capped or bare MnZnS NP in the presence of SARS-CoV-2 relative to the virus only control. Mean virus titers with SEM are shown for three independent experiments of four technical replicates each. Two-way ANOVA statistical analysis was performed on log transformed virus titer data using GraphPad Prism software. Statistically significant (*) reductions in virus titers were observed at 20 and 50 $\mu$g/mL of bare MnZnS NP and Cys-capped MnZnS NP, respectively. (B) Representative Vero E6 cell culture morphology by light microscopy after 48 h of exposure to 20 or 50 $\mu$g/mL of bare MnZnS NP or Cys-capped MnZnS NP, or with culture medium or SARS-CoV-2 virus only. Cytotoxic effects were observed at 50 $\mu$g/mL for both bare MnZnS NP and Cys-capped MnZnS NP.

interaction with ACE. Our results show that 3% or 5% MnZnS interaction with ACE significantly inhibited its biochemical activity, with the 3% material showing a dose−response trend with $IC_{50} \leq 50$ $\mu$g/mL. Dramatic inhibition is evident for the hydrolase class of enzymes, shown here for $\beta$-Gal and ACE. Whereas Cys-capping appeared to increase cell viability, this had no impact on antiviral activity, as the bare 3% MnZnS uncapped material showed the most viral specific activity with 1−2 log order inhibition of SARS-CoV-2 at a well-tolerated dose of 20 $\mu$g/mL. In particular, the impact that nanoparticle composites have on enzyme activity and the potential inhibition of SARS-CoV-2 hACE2 receptor shown here may extend to other types of hydrolases used by virus or cellular targets. The Mirkin group first published polyelemental nanoparticle composite libraries containing gold and silver doped with other physiological metals,[15] but the impact of the inclusion of zinc, manganese, and iron was not studied. More recent work however suggests that zinc-containing composi- tions can impact polymerase enzymes[16] which may be another important viral target, and it is notable that a gold-, silver-, and zinc-containing composite was recently shown to inhibit both influenza and SARS-CoV-2 viruses.[17] In conclusion, these data suggest the emergence of a new field of nanoparticle biochemical pharmacology and lead to further work to

translate this new class of enzyme inhibitors into animal and preclinical studies.

## ■ ASSOCIATED CONTENT

**Ⓢ Supporting Information**

The Supporting Information is available free of charge at https://pubs.acs.org/doi/10.1021/acsptsci.2c00041.

> Impact of ZnO nanosphere to nanorod ratios on luciferase biochemical activity; impact of iron oxide and iron and zinc containing composites on luciferase rapid kinetics; dose−response curves of 1% MnZnS nanoparticle on luciferase and $\beta$-galactosidase biochem- ical activity; UV curve of ACE at various 3% MnZnS ratios; MTT assay of 3% MnZnS capped cytotoxicity to NIH3T3 cells (PDF)

### Accession Codes

$\beta$-Galactosidase: UniProtKB A0A241QW94 (A0A241Q- W94_ECOLX). Angiotensin-converting enzyme 2: UniProtKB Q9BYF1 (ACE2_HUMAN). Angiotensin-converting enzyme: UniProtKB P12821 (ACE_HUMAN). Luciferase: UniProtKB P08659 (LUCI_PHOPY).

## ■ AUTHOR INFORMATION

### Corresponding Author

**Robert K. DeLong** — *Nanotechnology Innovation Center, Department of Anatomy and Physiology, Kansas State University, Manhattan, Kansas 66506, United States;* orcid.org/0000-0002-9568-7081; Phone: 785-532-6313; Email: robertdelong@vet.k-state.edu; Fax: 785-532-4953

### Authors

**Hanah Huber** — *Nanotechnology Innovation Center, Department of Anatomy and Physiology, Kansas State University, Manhattan, Kansas 66506, United States*

**Cesar Aparicio-Lopez** — *Nanotechnology Innovation Center, Department of Anatomy and Physiology, Kansas State University, Manhattan, Kansas 66506, United States*

**Abeera Bhatti** — *Nanotechnology Innovation Center, Department of Anatomy and Physiology, Kansas State University, Manhattan, Kansas 66506, United States*

**Ryan Swanson** — *Nanotechnology Innovation Center, Department of Anatomy and Physiology, Kansas State University, Manhattan, Kansas 66506, United States*

**Tej B. Shrestha** — *Nanotechnology Innovation Center, Department of Anatomy and Physiology, Kansas State University, Manhattan, Kansas 66506, United States*

**Natasha N. Gaudreault** — *Department of Diagnostic Medicine/Pathobiology, College of Veterinary Medicine, Kansas State University, Manhattan, Kansas 66506, United States*

Complete contact information is available at:
https://pubs.acs.org/10.1021/acsptsci.2c00041

## ■ ABBREVIATIONS

ACE, angiotensin converting enzyme; $\beta$-Gal, $\beta$-galactosidase; CD, circular dichroism; NR, nanorod; UV, ultraviolet; ZNP, zinc nanoparticle

## ■ REFERENCES

(1) Juliano, R. Nanomedicine: is the wave cresting? *Nat. Rev. Drug Discovery* **2013**, *12* (3), 171−172.

(2) Millagaha Gedara, N. I.; Xu, X.; DeLong, R.; Aryal, S.; Jaberi-Douraki, M. Global Trends in Cancer Nanotechnology: A Qualitative Scientific Mapping Using Content-Based and Bibliometric Features for Machine Learning Text Classification. *Cancers (Basel)* **2021**, *13* (17), 4417.

(3) Limo, M. J.; Sola-Rabada, A.; Boix, E.; Thota, V.; Westcott, Z. C.; Puddu, V.; Perry, C. C. Interactions between Metal Oxides and Biomolecules: from Fundamental Understanding to Applications. *Chem. Rev.* **2018**, *118* (22), 11118−11193.

(4) Gann, H.; Glaspell, G.; Garrad, R.; Wanekaya, A.; Ghosh, K.; Cillessen, L.; Scholz, A.; Parker, B.; Warner, M.; Delong, R. K. Interaction of MnO and ZnO nanomaterials with biomedically important proteins and cells. *J. Biomed Nanotechnol.* **2010**, *6*, 37−42.

(5) Barber, S.; Abdelhakiem, M.; Ghosh, K.; Mitchell, L.; Spidle, R.; Jacobs, B.; Washington, L.; Li, J.; Wanekaya, A.; Glaspell, G.; DeLong, R. K. Effects of nanomaterials on luciferase with significant protection and increased enzyme activity observed for zinc oxide nanomaterials. *J. Nanosci. Nanotechnol.* **2011**, *11*, 10309−10319.

(6) Thomas, S. E.; Comer, J.; Kim, M. J.; Marroquin, S.; Murthy, V.; Ramani, M.; Hopke, T. G.; McCall, J.; Choi, S. O.; DeLong, R. K. Comparative functional dynamics studies on the enzyme nano-bio interface. *Int. J. Nanomedicine.* **2018**, *13*, 4523−4536.

(7) Cha, S. H.; Hong, J.; McGuffie, M.; Yeom, B.; VanEpps, J. S.; Kotov, N. A. Shape-dependent biomimetic inhibition of enzyme by nanoparticles and their antibacterial activity. *ACS Nano* **2015**, *9* (9), 9097−9105.

(8) Ramani, M.; Mudge, M. C.; Morris, R. T.; Zhang, Y.; Warcholek, S. A.; Hurst, M. N.; Riviere, J. E.; DeLong, R. K. Zinc Oxide Nanoparticle-Poly I:C RNA Complexes: Implication as Therapeutics against Experimental Melanoma. *Mol. Pharmaceutics* **2017**, *14* (3), 614−625.

(9) DeLong, R. K.; Mitchell, J. A.; Morris, R. T.; Comer, J.; Hurst, M. N.; Ghosh, K.; Wanekaya, A.; Mudge, M.; Schaeffer, A.; Washington, L. L.; Risor-Marhanka, A.; Thomas, S.; Marroquin, S.; Lekey, A.; Smith, J. J.; Garrad, R.; Aryal, S.; Abdelhakiem, M.; Glaspell, G. P. Enzyme and Cancer Cell Selectivity of Nanoparticles: Inhibition of 3D Metastatic Phenotype and Experimental Melanoma by Zinc Oxide. *J. Biomed Nanotechnol.* **2017**, *13* (2), 221−231.

(10) DeLong, R. K.; Swanson, R.; Niederwerder, M. C.; Khanal, P.; Aryal, S.; Marasini, R.; Jaberi-Douraki, M.; Shakeri, H.; Mazloom, R.; Schneider, S.; Ensley, S.; Clarke, L. L.; Woode, R. A.; Young, S.; Rayamajhi, S.; Miesner, T.; Higginbotham, M. L.; Lin, Z.; Shrestha, T.; Ghosh, K.; Glaspell, G.; Mathew, E. N. Zn-based physiometa-composite nanoparticles: distribution, tolerance, imaging, and antiviral and anticancer activity. *Nanomedicine (Lond)* **2021**, *16* (21), 1857−1872.

(11) Wayu, M. B.; Spidle, R.; Devkota, T.; Deb, A. K.; Delong, R. K.; Ghosh, K.; Wanekaya, A. K.; Chusuei, C. C. Morphology of hydrothermally synthesized ZnO nanoparticles tethered to carbon nanotubes affects electrocatalytic activity for H2O2 detection. *Electrochim. Acta* **2013**, *97*, 99−104.

(12) DeLong, R. K.; Dean, J.; Glaspell, G.; Jaberi-Douraki, M.; Ghosh, K.; Davis, D.; Monteiro-Riviere, N.; Chandran, P.; Nguyen, T.; Aryal, S.; Russell Middaugh, C.; Chan Park, S.; Choi, Seong-O; Ramani, Meghana Amino/Amido Conjugates Form to Nanoscale Cobalt Physiometacomposite (PMC) Materials Functionally Delivering Nucleic Acid Therapeutic to Nucleus Enhancing Anticancer Activity via Ras-Trgeted Protein Interference. *ACS Appl. Bio Mater.* **2020**, *15* (12), e0243802.

(13) Reaz, M.; Haque, A.; Cornelison, D. M.; Wanekaya, A.; Delong, R.; Ghosh, K. Magneto-luminescent Zinc/Iron oxide core-shell nanoparticles with tunable magnetic properties. *Physica E: Low-dimensional Systems and Nanostructures* **2020**, *123*, 114090.

(14) Packer, M.; Poole-Wilson, P. A.; Armstrong, P. W.; Cleland, J. G.; Horowitz, J. D.; Massie, B. M.; Rydén, L.; Thygesen, K.; Uretsky, B. F. Comparative effects of low and high doses of the angiotensin-converting enzyme inhibitor, lisinopril, on morbidity and mortality in chronic heart failure. ATLAS Study Group. *Circulation* **1999**, *100* (23), 2312−2318.

(15) Chen, P.-C.; Liu, X.; Hedrick, J. L.; Xie, Z.; Wang, S.; Lin, Q.-Y.; Hersam, M. C.; Dravid, V. P.; Mirkin, C. A. Polyelemental nanoparticle libraries. *Science* **2016**, *352* (6293), 1565−1569.

(16) Gao, C.-H.; Mortimer, M.; Zhang, M.; Holden, P. A.; Cai, P.; Wu, S.; Xin, Y.; Wu, Y.; Huang, Q. Impact of metal oxide nanoparticles on in vitro DNA amplification. *PeerJ* **2019**, *7*, e7228.

(17) Chang, S.-Y.; Huang, K.-Y.; Chao, T.-L.; Kao, H.-C.; Pang, Y.-H.; Lu, L.; Chiu, C.-L.; Huang, H.-C.; Cheng, T.-J. R.; Fang, J.-M.; Yang, P.-C. Nanoparticle composite TPNT1 is effective against SARS-CoV-2 and influenza viruses. *Sci. Rep.* **2021**, *11*, 8692.